



# Damping ratio and power output prediction of an electromagnetic energy harvester designed through finite element analysis

Chung Ket Thein <sup>a,\*</sup>, Faruq Muhammad Foong <sup>a</sup>, Yi-Chung Shu <sup>b,\*</sup>

<sup>a</sup> School of Engineering and Physical Sciences, Heriot-Watt University, No. 1, Jalan Venna P5/2, Precinct 5, 62200, Malaysia

<sup>b</sup> Institute of Applied Mechanics, National Taiwan University, Taipei, 106, Taiwan, Republic of China

## ARTICLE INFO

### Article history:

Received 12 July 2018

Received in revised form 6 December 2018

Accepted 25 December 2018

Available online 28 December 2018

### Keywords:

Critical damped stress

Damping ratio

Finite element analysis

Electromagnetic vibration energy harvester

## ABSTRACT

This paper presents a novel and simplified method to predict the damping ratio and power output of a cantilever-based electromagnetic vibration energy harvester through finite element analysis. A strong relationship was determined between the mechanical damping of a structure and the resonant stress at the clamped end of the structure under critically damped condition, otherwise described as the critically damped stress. This relation was used as a basis to develop a material-specific damping stress equation. The equation was then integrated into FEA to analyse a certain electromagnetic vibration energy harvester design by considering the variation in damping and power output for every structural change. The effect of the phase difference on the power output of the electromagnetic harvester was also considered. The FEA design that recorded the highest power output prediction (11.1% higher than the initial structure) was then verified experimentally, displaying a good agreement with experimental results, recording an error of less than 5.0% for the amplitude and voltage evaluation and 8.0% for the power output assessment. Hence, this validates the accuracy of the proposed method in predicting not only the mechanical damping of regular cantilever beams, but also other cantilever beam-based structures.

© 2018 Elsevier B.V. All rights reserved.

## 1. Introduction

Research in vibration energy harvesting has been increasingly popular in the past decade due to its abundance from the surrounding [1]. The concept of vibration energy harvesting is to simply convert the mechanical energy of a vibrating structure into electrical power [2]. Normally, the harvester is designed to respond to external vibration input, hence utilising the theory of forced vibration. Many researches have designed these harvesters based on different mechanical-to-electrical conversion methods, with the two most common methods being piezoelectric conversion and electromagnetic induction. While electromagnetic harvesters generally consume more space than piezoelectric harvesters, their output current is several times higher due to low impedance [3].

Cantilever beam-based harvester designs are commonly studied due to its simplicity and effectiveness [4]. However, in an attempt to increase the power output and operational bandwidth of vibration energy harvesters, many researches have proposed different designs to address the problems [5–7]. A mathematical model is

usually desired for a proposed design as it provides the means to predict or optimise the performance of the design. To predict the power output of a vibration energy harvester, three main mathematical models are required which are the vibration response of the harvester, the power equation and the damping equations. The power equation is dependent on the type of transduction method used whereas the vibration response equation strongly relies on the properties of the structure. While there exist several mathematical models to describe the vibration response of a simple cantilever beam-based harvesters, it may be difficult to model the response of complex structures. In addition, the mathematical models derived even for simple cantilever beam vibrations are usually limited by the assumptions used. Hence, several researches have leaned towards the use of finite element analysis (FEA) as this method enables researchers to simulate the response of any vibrating structure with good accuracy [8–12]. The only drawback of this method is the time required to generate the results.

A typical vibration energy harvester have two sources of damping which are the electrical damping and the elastic damping. Many models have been developed to predict the electrical damping based on the chosen transduction method [13–16]. However, the main problem lies in modelling the mechanical damping equation of a structure. Despite the importance of mechanical damping, little is known about its characteristics. In any mathematical model or

\* Corresponding authors.

E-mail addresses: [ckthein@gmail.com](mailto:ckthein@gmail.com) (C.K. Thein), [yichung@iam.ntu.edu.tw](mailto:yichung@iam.ntu.edu.tw) (Y.-C. Shu).

FEA, this form of damping is usually an input parameter required to predict the response of the structure and is normally obtained from experiment. In a way, this actually defeats the purpose of using the mathematical model or FEA for predictions as one would have already performed the experiment to obtain the damping value. In an earlier study, Lazan [17] proposed a method to identify the mechanical damping of a structure based on its maximum stress response during vibration. He then developed a generalised damping stress equation to predict the damping of metals. A similar equation was also derived by Kume et al. [18]. Gounaris and Anifantis [19] applied Lazan's equation to the FEA method to predict the damping of beam like structures. The downside of this method is that the maximum stress parameter is also a function of damping. Hence, several iterations are required to obtain the correct damping, which may not be convenient for FEA applications. In addition, the damping stress equation developed by Lazan is a generalised equation of many different tested metals and may compromise in terms of accuracy due to its generalisation.

This paper presents a novel method to predict the mechanical damping of beam-based structures. The method emphasise on the use of the maximum critically damped stress parameter to identify damping. Since this parameter is obtained from the critically damped condition, it is not a function of damping. Hence, this method becomes more efficient for finite element analysis applications as only a single simulation is required to determine the unknown damping of a structure. This method depends on a material-specific empirical equation that was derived from experiments conducted using a simple cantilever beam structure. The proposed damping evaluation method was then applied to analyse the effects of structural change on the damping and power output of an electromagnetic vibration energy harvester through finite element analysis. The result from the analysis that predicted the highest power output was then compared to experiment to verify the validity of the proposed method.

## 2. Mean power output equations for electromagnetic vibration energy harvester

It was discussed earlier on the need of three mathematical models to fully describe the behaviour of a vibration energy harvester. If the FEA method was applied, two of the mathematical models can be eliminated as any common FEA software would be able to compute the corresponding results for a given input. These two models are the vibration response model and the power equation. Nevertheless, for a typical electromagnetic circuit, the induced root-mean square (RMS) voltage output at the load resistance,  $V_{rms}$  and its corresponding mean power output,  $P_{ave}$ , can be defined by the following equations [7].

$$V_{rms} = \frac{1}{\sqrt{2}} NBL_c v_c C_f \frac{R_L}{R_c + R_L} \quad (1)$$

$$P_{ave} = \frac{V_{rms}^2}{R_L} \quad (2)$$

where  $N$  is the number of turns of coil,  $B$  is the average strength of the magnetic field,  $L_c$  is the effective length of the coil,  $v_c$  is the relative cutting speed of the coil moving through the magnetic flux,  $C_f$  is the coil fill factor [20] and  $R_L$  is the load resistance and  $R_c$  is the coil resistance. Overall, only  $v_c$  is dependent on the mechanical properties of the vibrating structure. Therefore, it is more practical to apply these equations for the power evaluation of an electromagnetic harvester instead of simulating an electromagnetic FEA. Past literatures have showed that there exists an optimum  $R_L$  value,  $R_L^{opt}$ , that corresponds to the maximum power output [21–24]. This value is dependent on the properties of the coil, magnets and the vibrating structure itself. The cutting speed of the coil,  $v_c$ , is usu-

ally associated with the velocity of a vibrating structure and can be described by

$$v_c = \omega_s z \quad (3)$$

where  $\omega_s$  and  $z$  are the vibrating frequency and displacement of the vibrating structure. Normally, this term can easily be extracted from FEA. However, it is strongly dependent on the damping input provided in the simulation. The problem now lies in defining the damping of an electromagnetic harvester.

## 3. Damping equations

Normally, an electromagnetic harvester would have two main sources of damping which are the mechanical damping and the electromagnetic damping. These damping sources are usually evaluated separately, and summed up as a single damping value to define the total damping of the harvester.

### 3.1. Electromagnetic damping

The electromagnetic damping arises from the interaction between the induced eddy currents in the coil and the magnetic flux of the magnets, resulting in a force that retards motion [23]. For the  $n^{th}$  mode of vibration ( $n = 1, 2, 3, \dots$ ), this form of damping can be described by Eq. (4) as below

$$\xi_e^n = \frac{(NBL_c C_f)^2}{2m_{eff}\omega_n(R_c + R_L)} \quad (4)$$

where  $\xi_e^n$  is the  $n^{th}$  mode electromagnetic damping ratio,  $m_{eff}$  is the effective mass of the electromagnetic harvester and  $\omega_n$  is the  $n^{th}$  mode natural frequency of the harvester. Note that Eq. (4) can be derived from references [15,25] and the inclusion of the coil fill factor  $C_f$  is introduced for considering the total magnetic flux in a wounded coil [20]. The full derivation of Eq. (4) is provided in Appendix A.

### 3.2. Mechanical damping

The mechanical damping of a harvester is typically the sum of several damping component contributions such as external fluid damping, thermoelastic damping, stick-slip damping, squeeze damping and material damping [26–29]. While some of these dampings have been well modelled in the past, others such as material damping are still obscure. For most cases in optimization, the overall damping parameter is obtained once from experiment and is assumed constant regardless of the change in geometry and mass of the structure [30]. For macro sized structures ( $>100 \text{ mm}^3$ ), the material damping component is the main contributor towards mechanical damping whereas other forms of damping contributions are small enough to be assumed negligible [31]. Material damping arises from the internal frictional interaction between molecules and grain boundaries within a material during deformation, resulting in energy loss. Hence, material damping is highly dependent on the material properties of a structure.

Many damping models have been proposed to describe the damping of a structure such as Rayleigh damping viscous damping or coulomb damping [32]. However, the hysteretic and viscoelastic damping models are usually used to describe the material damping of a structure [33]. The major difference between these two damping models is their dependence on the driving frequency of the vibrating structure. Hysteretic damping model assumes that the damping capacity of a material is independent on its vibrating frequency whereas the viscoelastic damping model presumes otherwise. For most structural materials, the damping can be described by the hysteretic damping model [34]. Hysteretic damping is often

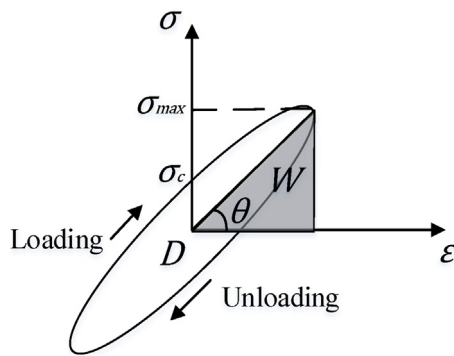


Fig. 1. Hysteretic damping model.

related to the nonlinear phenomenon during deformation. It was found that the deformation of a structure differs during loading and unloading, forming a closed loop in the stress-strain ( $\sigma$ - $\epsilon$ ) relation as shown in Fig. 1. The area bounded within this loop is described as the energy loss per unit volume, otherwise known as the damping energy.

Assuming a perfectly narrow elliptical hysteretic loop and considering Hooke's law where  $\tan\theta \approx \sigma/\epsilon = E$ , the damping energy,  $D$ , can be determined by

$$D = \frac{\pi\sigma_{max}\sigma_c \cos\theta}{\sin\theta} \approx \frac{\pi}{E} \sigma_{max}\sigma_c \quad (5)$$

where,  $E$  is the Young's modulus of the structure,  $\sigma_{max}$  is the maximum stress experienced in the structure and  $\sigma_c$  is the intersection between the hysteretic loop with the stress axis. A similar equation was also reported by Maghami [35]. The shaded area in Fig. 1 represents the maximum stored strain energy in the structure,  $W$ , which is described by

$$W = \frac{\sigma_{max}^2}{2E} \quad (6)$$

The loss factor of the structure then is defined as

$$\eta = \frac{D}{2\pi W} \approx \frac{\sigma_c}{\sigma_{max}} \quad (7)$$

where  $\eta$  is the loss factor of the structure. Lin and Zhu [36] stated that if proportional damping was assumed, the damping ratio of a structure is equal to half of its loss factor. Hence for first mode vibrations,

$$\zeta_1 \approx \frac{\sigma_c}{2\sigma_{max}} \quad (8)$$

where  $\zeta_1$  is the first mode damping ratio of the structure. For cases of a clamp-free cantilever beam,  $\sigma_{max}$  generally refers to the stresses at the clamped end of the beam. Lazan [17] showed that a strong relation exist between  $\sigma_{max}$  and  $\zeta_1$  of a beam structure. As stated earlier, the problem with defining damping in terms of  $\sigma_{max}$  is that  $\sigma_{max}$  is also a function of  $\zeta_1$ . Since a strong relation exist between  $\sigma_{max}$  and  $\zeta_1$ , it would not be wrong to assume that a strong relation would also exist between  $\sigma_c$  and  $\zeta_1$ . Nevertheless,  $\sigma_c$  have yet to be defined.

To evaluate  $\sigma_c$  for beam structures, a clamp-free cantilever beam with a tip mass placed on its free-end was considered as shown in Fig. 2, since this configuration is commonly applied in vibration energy harvesting applications. The  $L$  and  $h$  terms in Fig. 2 refers to the length and the thickness of the beam.

The transverse motion of the clamp-free cantilever beam subjected to a harmonic-base excitation at position  $x$  and time  $t$  can be described by the following equation.

$$z(x, t) = z_{abs}(x, t) - Y_0 e^{i\omega t} \quad (9)$$

where  $z(x, t)$  is the actual vertical displacement of the beam with respect to its clamped base,  $z_{abs}(x, t)$  is the absolute vertical displacement of the vibrating beam, and  $Y_0(t)$  and  $\omega$  are the vertical amplitude and driving frequency of the harmonic base excitation. For simplicity, the base excitation is assumed to be in harmonic motion. Assuming the length of the beam to be much larger than its thickness and width, the vibration response of the clamp-free beam under base excitation can be modelled using the Euler-Bernoulli beam theory. Using the method of separation of variables, the term  $z(x, t)$  can be separated into its spatial and temporal components.

$$z(x, t) = \sum_{n=1}^{\infty} \varphi_n(x) \eta_n(t) \quad (10)$$

where  $\varphi_n(x)$  is the cantilever beam's modal shape eigenfunction and  $\eta_n(t)$  is the regular-response function. These terms can be described as the following equations

$$\varphi_n(x) = P_n \left[ \cosh \frac{\beta_n}{L} x - \cos \frac{\beta_n}{L} x - \frac{B_n}{C_n} \left( \sinh \frac{\beta_n}{L} x - \sin \frac{\beta_n}{L} x \right) \right] \quad (11)$$

$$\eta_n(t) = \frac{\omega^2 Y_0 e^{i\omega t} F_n}{\omega_n^2 - \omega^2 + i2\zeta_n \omega_n \omega} \quad (12)$$

where  $P_n$ ,  $\beta_n$ ,  $B_n$ ,  $C_n$  and  $F_n$  are modal terms derived from the boundary conditions and the inertial effect of the beam mass system [37].  $\zeta_n$  corresponds to the modal mechanical damping ratio of the structure. Substituting Eqs. (11) and (12) into Eq. (10) and considering only the first mode parameters at resonance ( $\omega = \omega_1$ ) results in

$$z(x, t) = \frac{Y_0 e^{i\omega_1 t} \varphi_1(x)}{2\zeta_1} F_1 \quad (13)$$

The Euler-Bernoulli beam theory states that the bending stress experience by a beam at position  $x$  and  $y$  (along the thickness of the beam) can be defined as

$$\sigma = E y \frac{d^2 z(x)}{dx^2} \quad (14)$$

where  $\sigma$  is the stress experienced on the beam and  $y$  is the distance from the centre of the beam along the thickness. Substituting Eqs. (13) into (14) and considering the stresses on the clamped end surface of the beam ( $x = 0$  and  $y = h/2$ ) results in an equation

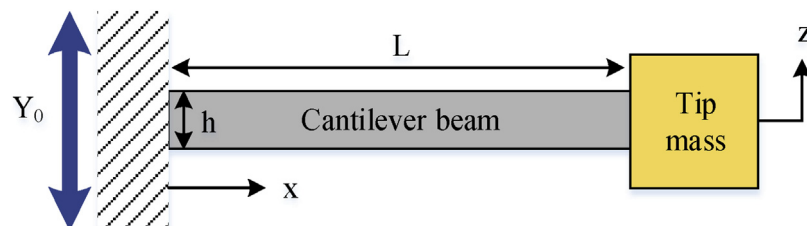


Fig. 2. Cantilever beam with a tip mass placed on the free-end of the beam.

**Table 1**

Material properties and thickness of the stainless steel beam used in experiment.

Material	$E$ (GPa)	$\rho$ ( $\text{kgm}^{-3}$ )	$h$ (mm)
Stainless Steel 316	180	7850	1.0

describing the maximum stress of a vibrating beam for first mode vibration

$$\sigma_{\max} = E \frac{h}{2} \frac{Y_0}{\zeta_1} \left( \frac{\beta_1}{L} \right)^2 P_1 F_1 \quad (15)$$

Relating Eqs. (15) to (8),  $\sigma_c$  can now be defined as Eq. (16) for cantilever beam structures under first mode vibrations.

$$\sigma_c = EhY_0 \left( \frac{\beta_1}{L} \right)^2 P_1 F_1 \quad (16)$$

Since  $\sigma_c$  is actually equal to twice the clamped-end stress value at resonance under critically damped condition ( $\zeta_1 = 1$ ), this term will be defined as the maximum critically damped stress. Eq. (16) also states that  $\sigma_c$  is not a function of damping. Therefore, defining damping in terms of  $\sigma_c$  may be better than  $\sigma_{\max}$  as no iterations would be required to solve for the damping.

Previous studies have emphasised on a strong relationship between  $\sigma_{\max}$  and  $\zeta_1$ . At this point, it is still unclear if  $\sigma_c$  would also display a similar trend with  $\zeta_1$ . Therefore, an experiment was conducted to compare the relation between  $\zeta_1$  and  $\sigma_c$  and  $\zeta_1$  and  $\sigma_{\max}$  for a stainless steel 316 cantilever beam with a tip mass. The specification of the beam is listed in Table 1 below.

One end of the stainless steel beam was clamped to a shaker to induce a base-excitation vibration. The beam was vibrated within a specified range of frequencies to make certain that resonance would occur. The maximum displacement of the free-end tip of the vibrating beam during resonance and its corresponding base-excitation amplitude were recorded. To ensure a consistency in the damping ratio results, the damping ratio was calculated using Eq. (13). The maximum stress and the maximum critically damped stress was then determined using Eqs (15) and (16). The experiment was repeated using different beam width (12–20 mm), beam length (60–100 mm), tip mass (9–60 g) and base excitation acceleration (0.5–7.0  $\text{ms}^{-2}$ ) to induce different damping and stress levels. Fig. 3 shows the comparison between the experimental result for  $\zeta_1$  against  $\sigma_c$  and  $\zeta_1$  against  $\sigma_{\max}$ . An empirical curve was fitted to the experimental data.

Visually, a stronger correlation can be observed between  $\zeta_1$  against  $\sigma_c$  in Fig. 3. The recorded coefficient of determination,  $R^2$ , for the correlation between  $\zeta_1$  against  $\sigma_c$  and  $\zeta_1$  against  $\sigma_{\max}$  were  $R^2 = 0.99$  and  $R^2 = 0.89$  respectively. In addition, the plot of  $\zeta_1$  against  $\sigma_{\max}$  displayed a more dispersed result as compared to  $\zeta_1$  against  $\sigma_c$ . This proves that the maximum critically damped stress

parameter is actually a better parameter to use to define the damping of a structure as it will result in a more accurate prediction for the damping of unknown structures. The proposed method here is not limited to stainless steel material and can be adapted to other material that exhibit a non-complex hysteretic damping behaviour. It is important to note that some structures may experience the maximum critically damped stress at a different location than the clamped end due to notches or sharp edge corners. In practical applications, small fillets are usually introduced in these regions to significantly reduce the stress. However, suggesting that damping would also reduce in relation to the decrease in stress at the following regions would be physically incorrect. In addition, stresses in sharp corners are local stresses which arise due to geometrical constraint, whereas stresses at the clamped end of a vibrating structure represents the global overall stress of the structure and is strongly related to the vibration amplitude and damping. Therefore, it is more appropriate to relate damping to the stress at the clamped end of a structure instead of the actual maximum stress at the said regions. Previous authors have also reported damping to be related to the clamp end of a vibrating structure based on their derivation of the damping stress equation [17–19]. Nevertheless, for a simple beam structure, the critically damped stress at the clamped end of the beam corresponds to the maximum critically damped stress. In this paper, the proposed mechanical damping ratio prediction method was integrated into FEA. Fig. 4 illustrates the flowchart of the overall process to determine the vibration response of a beam-based electromagnetic harvester using FEA.

The process begins by modelling the structure and assigning the necessary material properties and boundary conditions. The finite element model is then subjected to a modal analysis to determine its natural frequencies and effective mass. For complex structures, FEA provides an advantage in evaluating these parameters which may prove to be analytically difficult to obtain. Using the results from the modal analysis, the structure is then subjected to a harmonic analysis under critically damped conditions ( $\zeta_1 = 1$ ), and  $\sigma_c$  is taken as twice the maximum stress at the clamped end of the structure under resonance frequency. The damping stress equation is then applied to evaluate the structure's mechanical damping ratio. The electromagnetic damping ratio can be determined using the results from the simulated magnets in the FEA electromagnetic analysis and the structural modal analysis. The obtained damping values are then updated into the finite element model to simulate its true vibration response, which be substituted into Eqs. (1) and (2) to determine the power output of the harvester. This shows how the power output of the harvester is strongly related to the structure's damping capacity, as the damping of the structure determines its output vibration response.

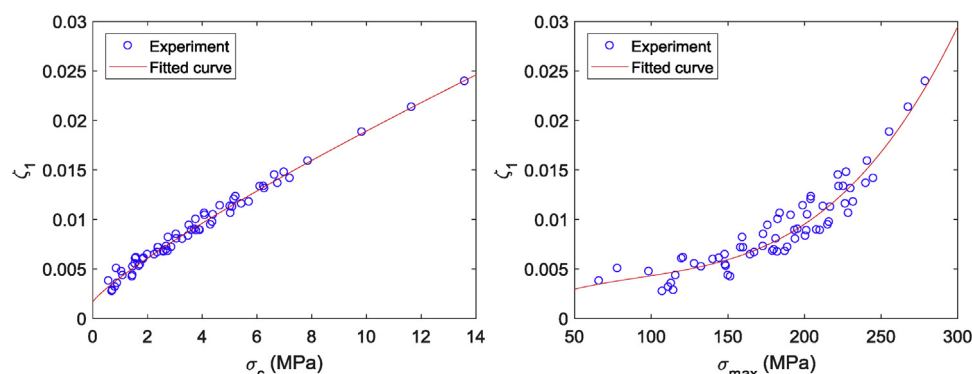
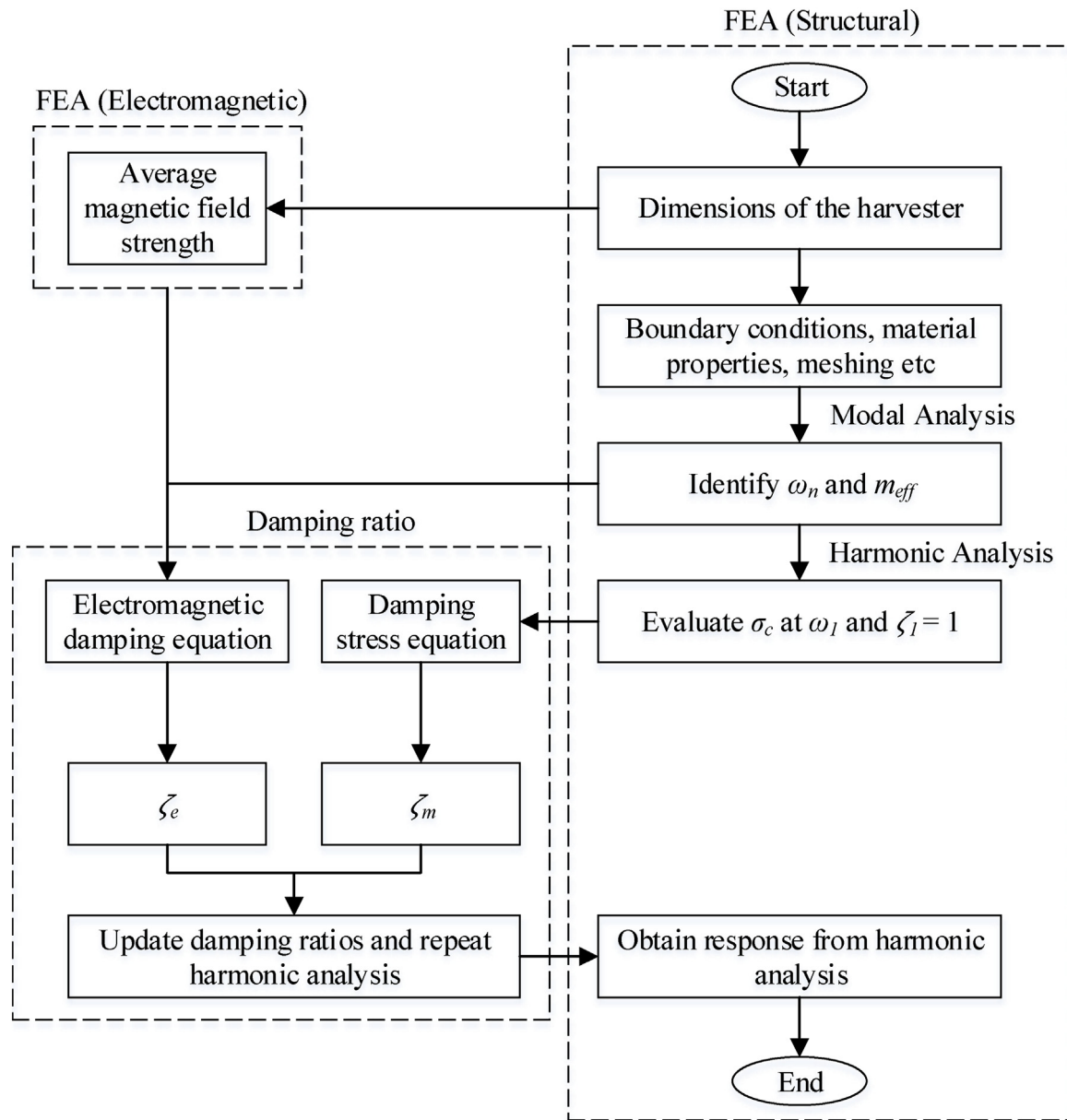


Fig. 3. Comparison among the relation between  $\zeta_1$  against  $\sigma_c$  and  $\zeta_1$  against  $\sigma_{\max}$ .



**Fig. 4.** Overall flow chart in estimating the vibration response of an electromagnetic harvester through FEA.

#### 4. Finite element modelling of an electromagnetic vibration energy harvester

In this paper, an electromagnetic vibration energy harvester design shown in Fig. 5 was analysed using FEA by considering the effect of structural change on the damping and power output prediction of the harvester. The design that recorded the highest power output was then verified through experiment. The design was initially proposed by Wu et al. and have the advantage of significantly reducing the first mode natural frequency and producing a larger bandwidth due to its multiple degree of freedom [38]. In addition, this structure can also validate the effectiveness of the presented mechanical damping evaluation method in predicting the mechanical damping ratio of a different cantilever beam-based structure rather than a regular cantilever beam. This design can be modelled as a three degree of freedom structure as shown by the schematic representation in Fig. 5. The terms  $m_1$ ,  $k_1$  and  $c_1$  in the schematic representation from Fig. 5 corresponds to the effective mass, stiffness and damping of the main frame and the

additional mass. Similarly,  $m_2$  and  $k_2$  relates to the coil beam, coil holder and coil wire whereas  $m_3$ ,  $k_3$  and  $c_3$  defines the magnet beam, magnet holder, magnets and steel plates. Nevertheless, the design was not modelled as so since the mechanical damping evaluation method developed in Section 3.2 requires the assessment of the structural stress. The harvester consists of a pair of magnets which are attached at the clamped end of the main frame with a set of coil wire extended from the free end of the main frame. The overall practical volume of the harvester measures by  $110 \times 60 \times 25$  mm (length  $\times$  width  $\times$  thickness). The materials used in the model are stainless steel 316 for the main frame, coil beam and magnet beam, four  $25 \times 10 \times 5$  mm of neodymium (NdFeB) magnets, a 0.25 mm diameter enamelled copper wire for the coil, and two  $5 \times 24 \times 22$  mm steel plates placed used to concentrate the magnetic field strength in air gap between the magnets [39].

The properties and dimensions of the coil holder, magnet holder, steel plates, magnets and coil were modelled based on the real available parts. Additional properties of the coil are tabulated in Table 2.

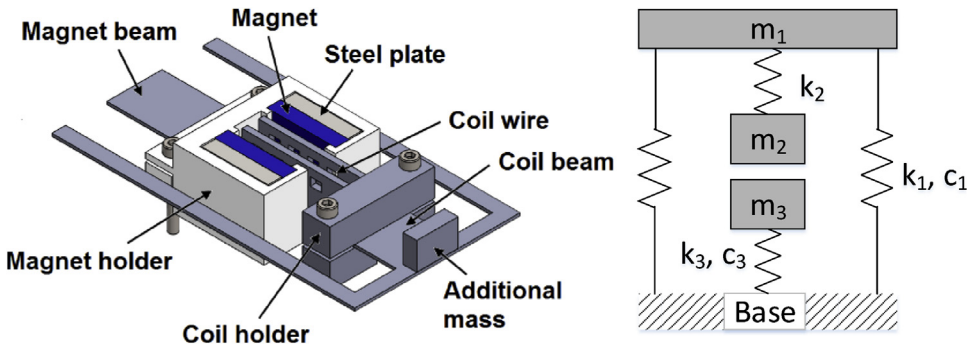


**Fig. 5.** Actual design and schematic spring-mass representation of the electromagnetic harvester.

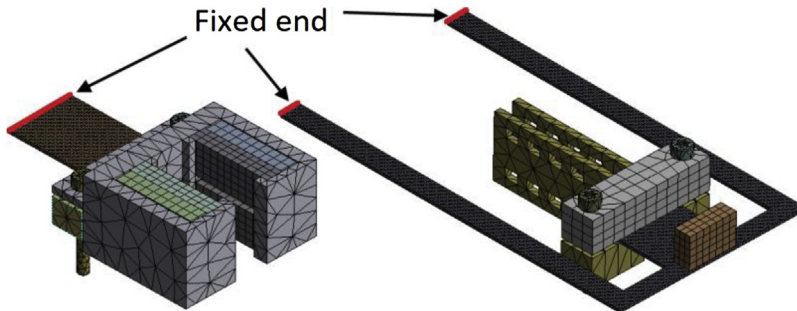


**Fig. 6.** Mesh and boundary conditions of the finite element model.

**Table 2**  
Properties of the coil section.

Parameters	$N$	$L_c$ (mm)	$C_f$	$R_c$ ( $\Omega$ )
Value	250	44	0.65	6.5

#### 4.1. FEA structural modelling

The design was modelled in ANSYS workbench 17.2 using a 10-node SOLID187 quadratic elements for round surface and a 20-node SOLID186 elements for the main frame with 0.5 mm element size. The total number of elements recorded for the finite element model is 31,039. A fixed boundary condition was applied on the clamped end of main frame and the magnet beam as seen in Fig. 6. Since the damping of the harvester would be evaluated based on the stresses on the main frame and the magnet beam, a denser mesh size was applied here. The magnet beam will have a different damping value than the main frame as it acts as a separate entity. Since the coil beam is actually part of the main frame, the mechanical damping of the coil beam and the main frame were evaluated as a single damping value.

It is important to note that the magnets and the coil were modelled as structural masses in ANSYS. Hence, there exist no electromagnetic interaction between them. In this paper, the vibration of the magnet beam and the main frame were simulated separately. A harmonic base acceleration input of  $4.905 \text{ ms}^{-2}$  was applied all the fixed boundary conditions to induce a base excitation motion. The mechanical damping of the structure was evaluated using the method presented in Fig. 4.

#### 4.2. FEA electromagnetic modelling

To calculate the electromagnetic damping, the magnets and the steel plates were simulated in CST Studio Suite 2017 using FEA to estimate its average magnetic field strength. The distance between the left and right magnets are 14 mm whereas the distance between

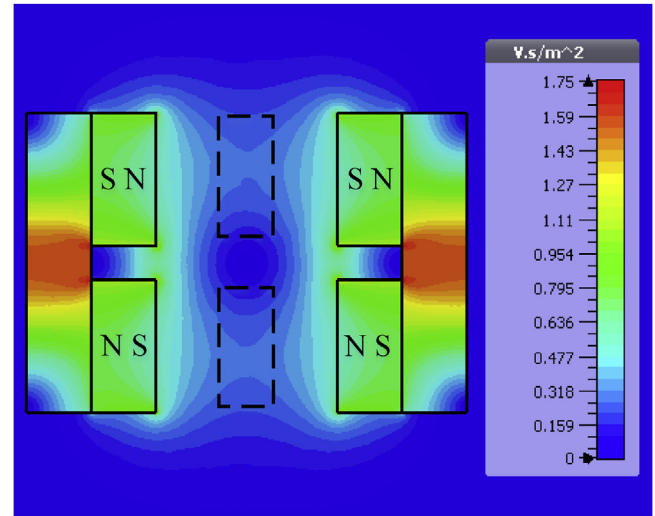


**Fig. 7.** Magnetic field strength contours of the permanent magnets and steel plates.

the top and bottom magnets are 5 mm. Fig. 7 describes the results of the FEA simulation. The orientation of the magnetic poles are inscribed onto each magnet. The black dashed boxes in Fig. 7 represents the areas covered by the coil in the magnetic field.

Based on the simulation results, the average magnetic field strength contacted by the coil was determined to be  $B = 0.26 \text{ T}$ . The optimum load resistance,  $R_L^{opt}$ , of the design was determined by simulating the design under different  $R_L$  values. A change in  $R_L$  value would produce a different electromagnetic damping ratio value for the same structure, hence resulting in a different vibrating amplitude. The power output of the harvester can then be calculated using Eqs. (1) and (2) based on the simulated amplitude. The  $R_L$  value that resulted in the highest power output was taken to be  $R_L^{opt}$  [40].

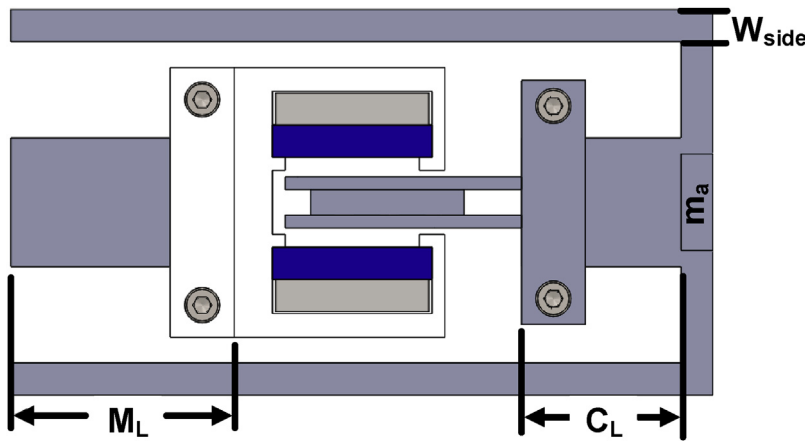


**Fig. 8.** Visual description on  $M_L$ ,  $C_L$ ,  $W_{side}$  and  $m_a$ .

**Table 3**  
Dimensions of Design 1.

Model	$C_L$ (mm)	$M_L$ (mm)	$W_{side}$ (mm)	$m_a$ (g)
Design 1	25	35	6.0	0.986

### 5. Analysis of the electromagnetic harvester design through FEA

A harmonic analysis was performed on the finite element model with the following dimensions shown in Table 3 using an input damping ratio of  $\zeta_1 = 1$  to determine the maximum critically damped stress at resonance. This design is the initial design of the harvester and will be designated as Design 1.

Here,  $M_L$  refers to magnet beam length,  $C_L$  refers to the coil beam length,  $W_{side}$  refers to the side width of the main frame and  $m_a$  is the mass of the additional mass added to the harvester as described by Fig. 8.

Since the vibration of the magnet beam and the main frame are independent to each other, the mechanical damping ratio of the magnet beam and the main frame needs to be evaluated separately. Using the empirical curve fit equation from Fig. 3, the mechanical damping ratio of the main frame and the magnet beam was determined to be  $1.5106 \times 10^{-2}$  and  $1.7370 \times 10^{-2}$  respectively. These damping values correspond to the first vibration mode. To estimate the mechanical damping of the second mode vibration for the main frame, the Rayleigh damping model was considered as shown by Eq. (17). This reason for this choice was because proportional damping was assumed earlier, and the Rayleigh damping model is commonly related to proportional damping [32]. The second mode vibration for the magnet beam was not considered due to its high natural frequency.

$$\xi_n = \frac{\gamma}{2\omega_n} + \frac{\mu\omega_n}{2} \quad (17)$$

where  $\xi_n$  represents the modal mechanical damping ratio and  $\gamma$  and  $\mu$  are constants corresponding to the mass and stiffness proportional damping. In many structural problems, the mass proportional damping can usually be ignored ( $\gamma = 0$ ) [41]. Hence, the second mode mechanical damping can be determined as follows

$$\xi_2 = \frac{\zeta_1\omega_2}{\omega_1} \quad (18)$$

As stated previously, the electromagnetic damping in the second vibration mode would be lower than the first vibration mode due to the increase in natural frequency. The same trend in electromagnetic damping at higher modes was also reported by Sadano et al. [42]. The modal damping was applied in ANSYS using the

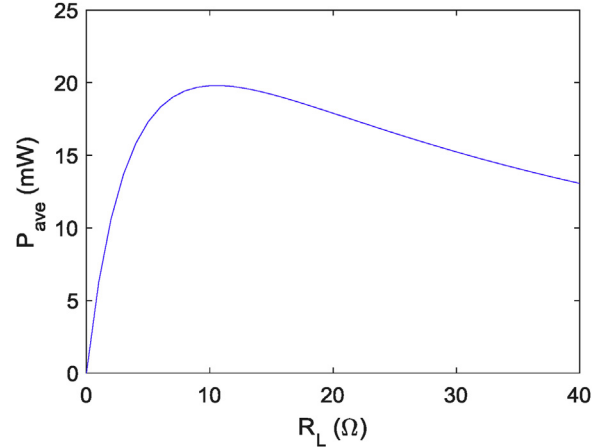


**Fig. 9.** Average simulated power against input load resistance for Design 1.

Rayleigh damping option by re-determining the  $\gamma$  and  $\mu$  constants from Eq. (17) based on the pre-determined total damping (mechanical damping + electromagnetic damping) of vibration mode 1 and 2. Note that at this point, the determination of the  $\gamma$  and  $\mu$  is only to ensure that the pre-determined total damping of vibration mode 1 and 2 is applied to the simulation, and would not be applicable for higher vibration modes. The effective mass of the main frame and the magnet beam obtained from the simulation was 32.4 g and 94.4 g. These values were used to determine the electromagnetic damping of both structures.

Design 1 was then simulated using different  $R_L$  values to determine  $R_L^{opt}$ . Since the magnets and the coil are both vibrating,  $R_L^{opt}$  was determined based on the structure that resulted in a higher individual power output (by assuming that their counter component is fixed to the base) to simplify analysis. Although the power output of the whole design would depend on the relative motion between the two components, the peaks in the overall power output would still correspond to the maximum individual power outputs of the vibrating coil and the magnets. Fig. 9 shows the curve of the average simulated power against the input load resistance value for Design 1.

$R_L^{opt}$  was determined to be  $10.5 \Omega$ , resulting in an electromagnetic damping ratio value of  $1.8630 \times 10^{-2}$  and  $0.4110 \times 10^{-2}$  for the main frame and the magnet beam. The harmonic analysis was then repeated using the determined mechanical and electromagnetic damping ratio values within a frequency range of 20 Hz–50 Hz. The results recorded maximum actual amplitude of 2.25 mm on the top surface of the coil and 2.15 mm on the top

surface of the magnets under first mode resonance. The first and second mode natural frequency of the main frame was determined to be 26.8 Hz and 60.6 Hz respectively, where the fundamental natural frequency of the magnet beam was 41.7 Hz. The result describes a 33.8 Hz difference between the first and second mode natural frequency of the main frame. It is worth to mention that Wu et al. [38] recorded an anti-phase motion between the coil beam and the main frame when using a similar model. However, the simulation results of the Design 1 did not record such occurrence which may be due to different material and geometry application. Within the given frequency range, Design 1 recorded two significant peaks in its power output prediction corresponding to the first vibration mode of the main frame and the magnet beam, with a magnitude of 9.0 mW and 19.7 mW respectively. The presence of distinct peaks are commonly observed in vibrating systems with more than a single degree of freedom [43]. The second vibration mode of the main frame did not contribute to the power output of the design as its natural frequency was beyond the set frequency range.

The design was then modified by adjusting the length of the magnet beam and the coil beam while maintaining the same practical volume of the design (110 mm × 60 mm × 25 mm). The distance between the magnets and coil was also fixed. The first mode natural frequency of the main frame in the altered designs was tuned to be equal to the initial design by increasing the mass of the additional mass or by increasing the side width of the main frame inwards or both. The natural frequency of the magnet beam was not tuned in any manner due to the large frequency gap between each design making it practically difficult. For each modified design, the modal mechanical damping ratio for the main frame and the magnet beam was re-evaluated using the proposed method from Section 3 and Eq. (3). The optimum load resistance for whole structure was also reassessed. Tables 4 and 5 tabulates the parameters of the initial and modified main frame and magnet beams for all designs.

Simulation results showed that the maximum critically damped stress for Design 4 was not located at the clamped end of the main frame as seen in Fig. 10. Nevertheless, the mechanical damping was

evaluated base on the critically damped stress at the clamped end due to the reasons discussed earlier.

The magnet beam length was not decreased beyond 10 mm as this length in the minimum beam length required to clamp the magnet holder. Similarly, the coil beam length was not decreased further than 10 mm as well. Fig. 11 illustrates the phase angle ( $\varphi$ ) and the actual amplitude (z) of the coil and the magnets.

It can be seen that the actual amplitude and phase angle of the magnets for Designs 2, 3 and 4 are significantly lower than the coil amplitude within the given frequency range. The phase angle of Designs 0 and 1 are exactly the same. Due to the vibration of both the coil and the magnet, the output voltage or power of the harvester would be dependent on the relative velocity of the vibrating coil with respect to the vibrating magnet. Under the same frequency, Eq. (3) shows that this velocity can be defined in terms of relative amplitude. The relative amplitude of the vibrating component is determined by

$$z_{rel} = [z_{coil}^2 + z_{mag}^2 - 2z_{coil}z_{mag}\cos(\Delta\varphi)]^{0.5} \quad (19)$$

where

$$\Delta\varphi = |\varphi_{coil} - \varphi_{mag}| \quad (20)$$

where if  $z_{rel}$  is the relative amplitude between the coil and the magnets,  $\Delta\varphi$  is the phase difference between the coil and the magnets,  $z_{coil}$  and  $\varphi_{coil}$  is the actual amplitude and phase angle of the vibrating coil and  $z_{mag}$  and  $\varphi_{mag}$  represent the similar parameter for the magnets.

No occurrence of anti-phase was recorded for all modified designs. Table 4 shows that increasing the coil beam length results in a decrease the electromagnetic damping of the harvester due to the increase in effective mass. Moreover, the natural frequency of the second vibration mode decreases when the coil beam length was increased. There was no clear relationship observed between each design in terms of the harvester's mechanical damping ratio. Fig. 12 describes the relative amplitude and the phase difference between the vibrating coil and magnets for all designs, which were

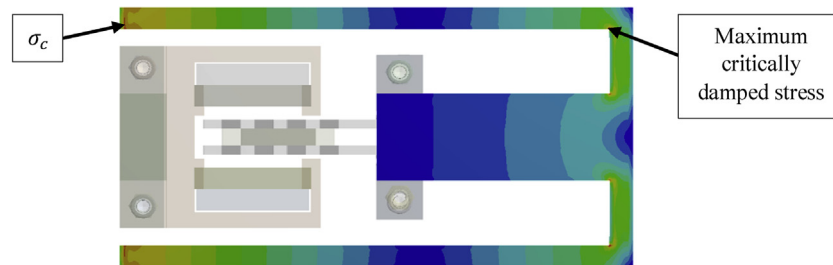


**Fig. 10.** Correct evaluation on the critically damped stress parameter for mechanical damping determination.

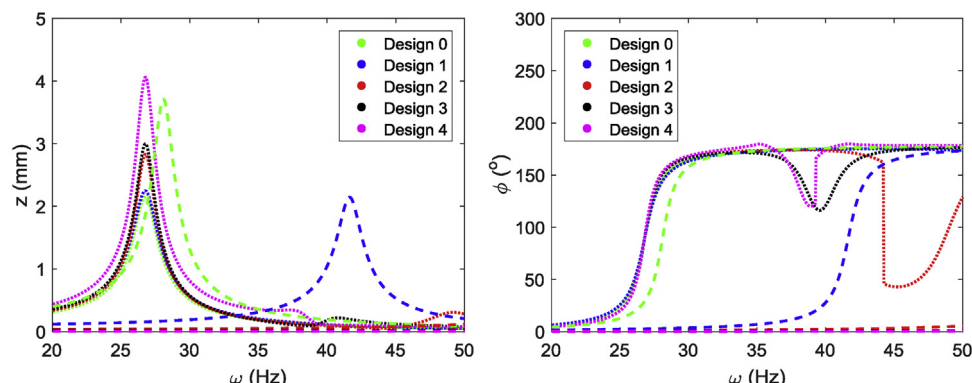


**Fig. 11.** Actual amplitude and phase angle for Designs 0–4. The dotted lines (..) represent the coil and the dashed lines (—) are the magnets.

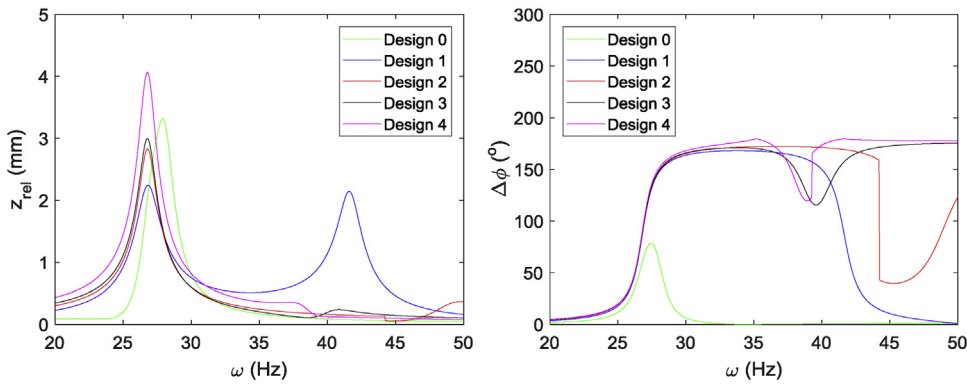


**Fig. 12.** Relative amplitude and phase difference of Designs 0–4.

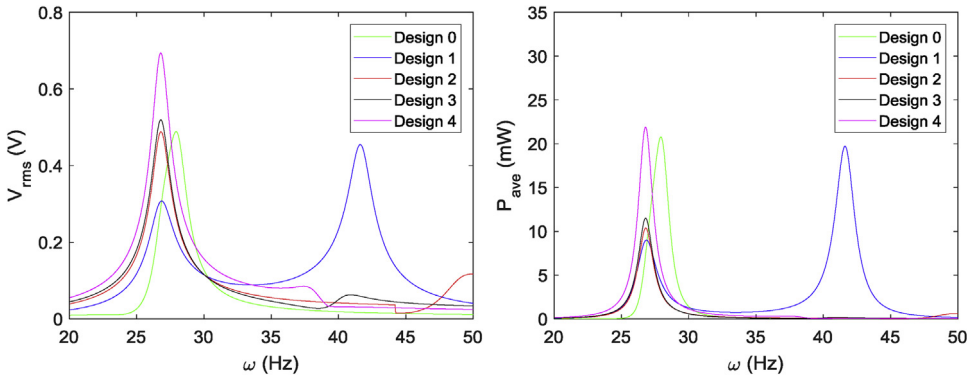


**Fig. 13.** RMS voltage and mean power output of the Designs 0–4.

**Table 4**

Design parameters of the initial and modified main frame of the harvester.

Model	Design 0	Design 1	Design 2	Design 3	Design 4
$C_L$ (mm)	10	25	35	45	50
$M_L$ (mm)	50	35	25	15	10
$W_{side}$ (mm)	7.2	6.0	5.5	5.0	5.0
$m_a$ (g)	0.579	0.986	1.169	0.758	0.000
$\omega_1$ (Hz)	26.8	26.8	26.8	26.8	26.8
$\omega_2$ (Hz)	80.5	60.6	49.0	40.3	38.5
$\sigma_c$ (MPa)	6.0160	7.0842	7.4290	7.4858	6.8478
$m_{eff}$ (g)	30.7	32.4	33.6	35.1	35.2
$R_L^{opt}$ ( $\Omega$ )	11.5	10.5	23.0	23.5	22.0
$\zeta_1 (\times 10^{-2})$	1.3324	1.5106	1.5675	1.5768	1.4714
$\zeta_e^1 (\times 10^{-2})$	1.8587	1.8630	1.0362	1.0091	1.0229
$\zeta_2 (\times 10^{-2})$	4.0009	3.4158	2.8660	2.3711	2.1138
$\zeta_e^2 (\times 10^{-2})$	0.6182	0.8239	0.5662	0.6704	0.7120

**Table 5**

Design parameters of the initial and modified magnet beam of the harvester.

Model	Design 0	Design 1	Design 2	Design 3	Design 4
$\omega_1$ (Hz)	28.1	41.7	58.9	95.9	140.5
$\sigma_c$ (MPa)	10.8372	8.4664	6.4918	4.6074	3.3402
$m_{eff}$ (g)	98.8	94.4	90.0	83.2	77.5
$\zeta_1 (\times 10^{-2})$	2.1157	1.7370	1.4120	1.0908	0.8663
$\zeta_e^1 (\times 10^{-2})$	0.5503	0.4110	0.1759	0.1189	0.0828

calculated using Eqs. (19) and (20). The RMS voltage and mean power outputs of Designs 0 to 4 were calculated using Eqs. (1) to (3) and plotted in Fig. 13. Compared to all the designs, Design 4 displayed the highest relative amplitude, recording a 81.0% increase as compared to Design 1. Consequently, this resulted in the highest power output generated by Design 4, being 11.1% higher than Design 1. In addition, Design 4 also recorded a smaller frequency for the second vibration mode. Nevertheless, the contribution from

the second vibration mode in terms of power output was small and not very significant. The contribution from the magnet vibration in Design 4 was also insignificant due to its high natural frequency and very low vibration amplitude for the given frequency range. Hence, this causes the bandwidth of Design 4 to be significantly lower than Design 1.

Design 4 recorded the lowest first modal damping for both the main frame and the magnet beam as compared to all designs. Normally, concluding that a harvester with the lowest damping would produce the maximum power is too simplistic as there are many other parameters that need to be considered, although this inference was observed in Fig. 13 [44–46]. However, the concluding statement holds true for the case of linear electromagnetic single degree of freedom systems if the natural frequency, phase angle, inertial effects and electromagnetic factors are alike. Since the harvester design analysed in this study causes both the coil and the magnets to vibrate, it would be more accurate relate the relative amplitude of the harvester to its resonant power output. In this case, it was observed that the increase in relative amplitude for Designs 0–4 under the first mode natural frequency of the main frame corresponded to the increase in the Design's maximum power output at this frequency.

It is worth to mention that the maximum relative amplitude of Design 0 is 10.6% lower and its maximum magnet actual amplitude. This significant drop in amplitude is attributed to the small phase difference between the coil and the magnets of Design 0 near its respective natural frequencies. In addition, the small amplitude difference between the coil and the magnets also contributed to the decrease in relative amplitude. This also caused the relative amplitude of Design 0 below its first resonance mode to be significantly deteriorated as compared to other designs. This shows that under the condition of a small phase difference, it is more desir-

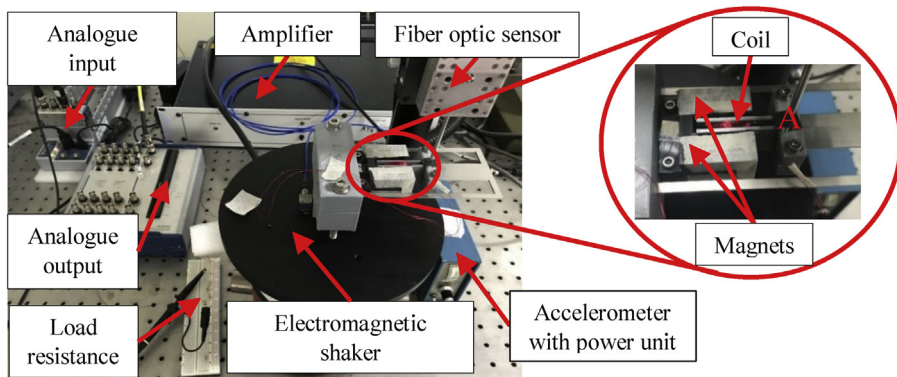


**Fig. 14.** Experiment setup of the proposed electromagnetic vibration energy harvester.

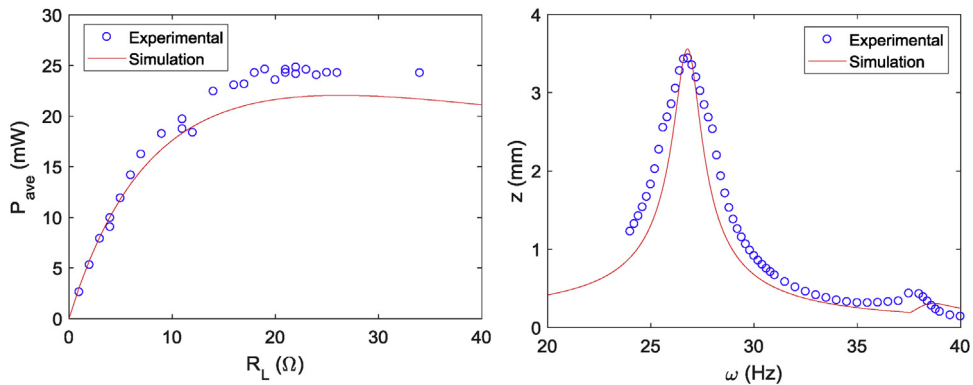


**Fig. 15.** Comparison between FEA simulation and experimental average power against load resistance and actual amplitude at location A.

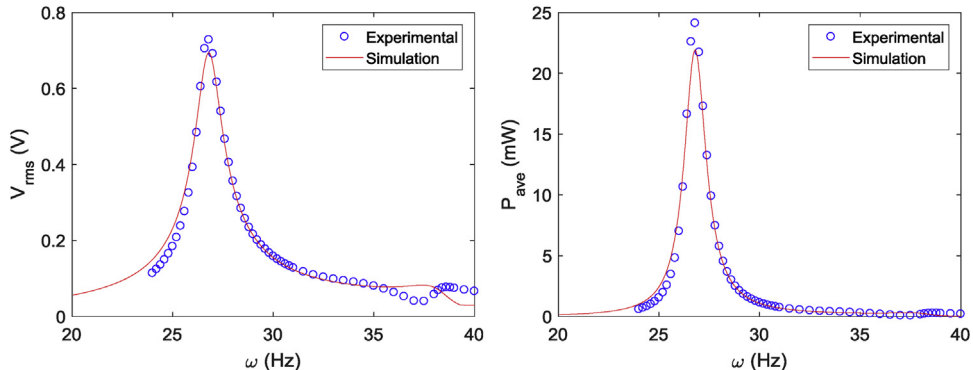


**Fig. 16.** Comparison between FEA simulation and experimental RMS voltage and mean power output at the load resistance.

able to maximise the amplitude difference between the coil and the magnets.

Overall, it is difficult to justify the best design among Designs 0–4. However, it can be concluded for the proposed harvester that under the same fundamental natural frequency, maximising the coil beam length will result in the maximum power output whereas compromising the coil beam length for magnet beam length can improve its operational bandwidth. For this study, Design 4 was chosen to be verified with experiment due to its highest power output.

## 6. Experimental verification

The main frame for Design 4 was manufactured and tested experimentally. The prototype was fixed onto a Data Physics (V20) electromagnetic shaker as shown in Fig. 14. The shaker was vibrated

using an analogue output NI-USB 6341 frequency generator with a feedback system established using an accelerometer (500 mV/g). The frequency generator and the feedback accelerometer was connected to an analogue input NI9229 data acquisition (DAQ) card. The DAQ card was linked to the computer and controlled through LabVIEW. The displacement of the vibrating coil was separately measured and recorded using a Fiber Optic MTI 2100 Fotonic Sensor. In the experiment, the coil displacement was measured at location A as shown in the zoomed in section of Fig. 14. Consequently, the amplitude readings at point A was also extracted from the FEA simulation.

The prototype was vibrated using the same base acceleration input as the simulation, which was  $4.905 \text{ ms}^{-2}$ . Experimental results recorded 26.8 Hz and 37.5 Hz as the corresponding first and second mode natural frequency of the prototype. These results show a good agreement between the simulation and the experi-

ment with less than 3.0% error. Fig. 15 shows that the comparison between the simulation and the experiment result for the average power against load resistance and actual amplitude of the coil at location A. Fig. 16 displays the comparison of between experimental and simulation results for the RMS voltage output and mean power output at the load resistance. Again, a good agreement can be observed in both figures especially under the first vibration mode. Therefore, this verifies the effectiveness of the damping prediction method presented in this paper and highlights the success of the presented mechanical damping evaluation method in predicting the mechanical damping ratio of a complex cantilever beam-based structure. A higher error was recorded at the second vibration mode peak as compared to the first peak which may due to the use of the Rayleigh damping approximation. In previous works, some authors would assume a constant damping parameter when optimising or evaluating a vibration energy harvester [30,47], regardless of its parametric changes. If the same method was applied in this study, it would inevitably lead to larger discrepancies between the experiment and simulation result. Hence, this shows the importance of properly defining the damping of a structure to improve the accuracy in analytical predictions.

## 7. Conclusion

A novel method in predicting the mechanical damping ratio and power output of an electromagnetic vibration energy harvester was proposed in this paper. It was found that based on the hysteretic damping model, it was possible to relate the damping of a structure to its critically damped stress. An experiment was performed to verify the relation between the mechanical damping ratio of stainless steel cantilevers beams with the critically damped stress. Results displayed a strong agreement between these two parameters, recording a high coefficient of determination of  $R^2 = 0.99$ . In addition, the critically damped stress parameter is independent of damping, making it more suited for FEA applications. The empirical damping relation derived from the experiment was implemented into FEA to analyse the damping and power output of a certain vibration energy harvester design. The result that predicted the highest power output was then manufactured, experimentally tested and compared to the FEA simulation result. A strong agreement was recorded between the simulation and the experimental results in terms of natural frequency, vibration amplitude and mean power output amounting to an error of less than 8.0%. Hence, this confirms the effectiveness of the proposed method presented in this work. Since the structure of the harvester analysed in this study represents a complex cantilever beam-based structure, it shows that the damping prediction method proposed here is not only valid for regular cantilever beams but can be applied for cantilever beam-based vibration energy harvesters or structures. However, the electrical damping ratio must be modified if other mechanical to electrical conversion methods are used. Based on the damping evaluation method developed here, future works will consider a study in shape and sizing optimisation of vibration energy harvesters using FEA.

## Acknowledgements

The authors would like to acknowledge the funding body from the Taiwan Fellowship program, Ministry of Foreign Affairs in Taiwan for funding this research and the partial support from National Taiwan University and Ministry of Science and Technology under Grant Nos 105-2923-E-002-006-MY3 and 105-2221-E-002-028-MY3.

## Appendix A

Appendix A describes the derivation of the electromagnetic damping ratio equation as illustrated by Eq. (4). From Faraday's law of electromagnetism, the induced voltage of an electromagnetic circuit

$$V = B_T L_c v_c \quad (A1)$$

where  $V$  is the induced voltage and  $B_T$  is the total magnetic flux in the coil. Owens and Mann defined the total magnetic flux in a wounded coil as  $B_T = NBC_f$  [20]. Hence,

$$V = NBC_f L_c v_c \quad (A2)$$

The power generated in the coil,  $P$ , can be related to the electromagnetic damping coefficient,  $C_e$ , as [15,25]

$$P = C_e v_c^2 \quad (A3)$$

According to ohm's law, the power output can also be related to the induced voltage by

$$P = \frac{1}{R_c + R_L} V^2 = \frac{1}{R_c + R_L} (NBC_f L_c v_c)^2 \quad (A4)$$

Therefore,

$$C_e = (NBC_f L_c)^2 \frac{1}{R_c + R_L} \quad (A5)$$

and the electromagnetic damping ratio is thus equal too

$$\zeta_e^n = \frac{C_e}{2m_{eff}\omega_n} = \frac{(NBL_c C_f)^2}{2m_{eff}\omega_n (R_c + R_L)} \quad (A6)$$

Note that the electromagnetic damping coefficient,  $C_e$ , is constant for a fixed electromagnetic component. It is independent of the structures modal parameters. This means that for any vibration mode,  $C_e$  remains the same. Therefore for the same structural geometry, the modal electromagnetic damping ratio,  $\zeta_e^n$ , only depends on the modal natural frequency of the structure. On the other hand, the mechanical damping coefficient is strongly dependent on the structure's modal parameter. The Rayleigh damping model provides a means to estimate the mechanical damping coefficient for different modes.

## References

- [1] S. Ju, C.H. Ji, Impact-based piezoelectric vibration energy harvester, *Acs Appl. Energy Mater.* 214 (2018) 139–151.
- [2] C.B. Williams, R.B. Yates, Analysis of a micro-electric generator for microsystems, *Sens. Actuators A: Phys.* 52 (1996) 8–11.
- [3] E.M. Nia, N.A. Wan Abdullah Zawawi, B. Singh, M. Singh, A review of walking energy harvesting using piezoelectric materials, *IOP Conf Ser: Mater. Sci. Eng.* 291 (2017), 012026.
- [4] H. Fu, G. Chen, N. Bai, Electrode coverage optimization for piezoelectric energy harvesting from tip excitation, *Sensors* 18 (2018) 804.
- [5] H.S. Kim, J.W. Kim, S.B. Park, Y.J. Choi, Design of serial linkage-type vibration energy harvester with three resonant frequencies, *Smart Mater. Struct.* 26 (11) (2017), 115030.
- [6] W. Yang, S. Towfighian, A hybrid nonlinear vibration energy harvester, *Mech. Syst. Signal Process.* 90 (2017) 317–333.
- [7] F.M. Foong, C.K. Thein, B.L. Ooi, D. Yurchenko, Increased power output of an electromagnetic vibration energy harvester through anti-phase resonance, *Mech. Syst. Signal Process.* 116 (2019) 129–145.
- [8] A. Kumar, A. Sharma, R. Kumar, R. Vaish, V.S. Chauhan, Finite element analysis of vibration energy harvesting using lead-free piezoelectric materials: a comparative study, *J. Asian Ceram. Soc.* 2 (2) (2014) 138–143.
- [9] D. Gedeon, S.J. Rupitsch, Finite element based system simulation for piezoelectric vibration energy harvesting devices, *J. Intell. Mater. Syst. Struct.* 29 (7) (2018) 1333–1347.
- [10] C. Marqui Junior, A. Erturk, D.J. Inman, An electromechanical finite element model for piezoelectric energy harvester plates, *J. Sound Vib.* 327 (2009) 9–25.
- [11] C.K. Thein, B.L. Ooi, J.S. Liu, J.M. Gilbert, Modelling and optimization of a bimorph piezoelectric cantilever beam in an energy harvesting application, *J. Eng. Sci. Tech.* 11 (2) (2016) 212–227.

- [12] P.H. Wu, Y.C. Shu, Finite element modelling of electrically rectified piezoelectric energy harvesters, *Smart Mater. Struct.* 24 (2015), 094008.
- [13] Y. Tan, Y. Dong, X. Wang, Review of MEMS electromagnetic vibration energy harvester, *J. Microelectromech. Syst.* 26 (1) (2017) 1–15.
- [14] H. Shen, J. Qiu, M. Bals, Vibration damping as a result of piezoelectric energy harvesting, *Sens. Actuators A: Phys.* 169 (2011) 178–186.
- [15] V.R. Challa, M.G. Prasad, F.T. Fisher, A coupled piezoelectric-electromagnetic energy harvesting technique for achieving increased power output through damping matching, *Smart Mater. Struct.* 18 (2009), 095029.
- [16] Y.C. Shu, I.C. Lien, Efficiency of energy conversion for a piezoelectric power harvesting system, *J. Micromech. Microeng.* 16 (2006) 2429–2438.
- [17] B.J. Lazan, *Damping of Materials and Members in Structural Mechanics*, Pergamon Press, London, 1968.
- [18] Y. Kume, F. Hashimoto, S. Maeda, Material damping of cantilever beams, *J. Sound Vib.* 80 (1) (1982) 1–10.
- [19] G.D. Gounaris, N.K. Anifantis, Structural damping determination by finite element approach, *Comp. Struct.* 73 (1999) 445–452.
- [20] B.A.M. Owens, P.M. Brian, Linear and nonlinear electromagnetic coupling models in vibration-based energy harvesting, *J. Sound Vib.* 331 (2012) 922–937.
- [21] B. Yang, C. Lee, W. Xiang, J. Xie, J.H. He, R.K. Kotlanka, S.P. Low, H. Feng, Electromagnetic energy harvesting from vibrations of multiple frequencies, *J. Micromech. Microeng.* 19 (2009), 035001.
- [22] C.T. Saha, T. O'Donnell, H. Loder, S. Beeby, J. Tudor, Optimization of an electromagnetic energy harvesting device, *IEEE Transl. J. Magn. Jpn.* 42 (10) (2006) 3509–3511.
- [23] W.C. Tai, L. Zuo, On optimisation of energy harvesting from base-excited vibration, *J. Sound Vib.* 411 (2017) 47–59.
- [24] E. Arroyo, A. Badel, Electromagnetic vibration energy harvesting device optimization by synchronous energy extraction, *Sens. Actuators A: Phys.* 171 (2) (2011) 266–273.
- [25] M. El-hami, P. Glynne-Jones, N.M. White, M. Hill, S.P. Beeby, E. James, A.D. Brown, J.N. Ross, Design and fabrication of a new vibration-based electromechanical power generator, *Sens. Actuators A: Phys.* 92 (2001) 335–342.
- [26] H. Nouira, E. Folt, L. Hirsinger, S. Ballandras, Investigation of the effects of air on the dynamic behaviour of a small cantilever beam, *J. Sound Vib.* 305 (2007) 243–260.
- [27] R. Lifshitz, M.L. Roukes, Thermoelastic damping in Micro- and nano-mechanical systems, *Phys. Rev. B* 61 (8) (2000) 5000–5009.
- [28] C. Zhang, G. Xu, Q. Jiang, Analysis of the air-damping effect on a micromachined beam resonator, *Math. Mech. Solids* 8 (2003) 215–225.
- [29] F. Ohlsson, E. Svensson, C. Rusu, Modelling squeeze film damping in packaged energy harvesters, in: European Conference on Circuit Theory and Design (ECCTD) Conference, 2015.
- [30] S.J. Roundy, Energy Scavenging for Wireless Sensor Nodes With a Focus on Vibration to Electricity Conversion, PhD thesis, 2003.
- [31] J.B. Alblas, A note on the theory of thermoelastic damping, *J. Thermal Stress* 4 (1981) 333–355.
- [32] S. Adikari, Damping Models for Structural Vibrations, PhD thesis, 2000.
- [33] V. Arora, Structural damping identification method using normal FRFs, *Inter. J. Solids Struct.* 51 (2014) 133–143.
- [34] J.S. Whittier, Hysteretic damping of structural materials under biaxial dynamic stresses, *Exp. Mech.* 2 (11) (1962) 312–328.
- [35] S. Maghami, Silica-filled Tire Thread Compounds: an Investigation Into the Viscoelastic Properties of the Rubber Compounds and Their Relation to Tire Performance, PhD thesis, 2016.
- [36] R.M. Lin, J. Zhu, On the relationship between viscous and hysteretic damping models and the importance of correct interpretation for system identification, *J. Sound Vib.* 325 (2009) 14–33.
- [37] A. Erturk, D.J. Inman, On mechanical modeling of cantilevered piezoelectric vibration energy harvesters, *J. Intell. Mater. Syst. Struct.* 19 (2008) 1311–1325.
- [38] H. Wu, L. Tang, Y. Yang, C.K. Soh, Development of a broadband nonlinear two-degree-of-freedom piezoelectric energy harvester, *J. Intell. Mater. Syst. Struct.* 25 (4) (2014) 1875–1889.
- [39] B.L. Ooi, J.M. Gilbert, Design of wideband vibration-based electromagnetic generator by means of dual-resonator, *Sens. Actuators A: Phys.* 213 (2014) 9–18.
- [40] S.P. Beeby, R.N. Torah, M.J. Tudor, P. Glynne-Jones, T. O'Donnell, C.R. Saha, S. Roy, A micro electromagnetic generator for vibration energy harvesting, *J. Micromech. Microeng.* 17 (2007) 1257–1265.
- [41] C. Cai, H. Zheng, M.S. Khan, K.C. Hung, Modeling of material damping properties in ANSYS, in: ANSYS Conf., 2002.
- [42] H. Sodano, J.S. Bae, D.J. Inman, W.K. Belvin, Concept and model of eddy current damper for vibration suppression of a beam, *J. Sound Vib.* 288 (2005) 1177–1196.
- [43] H.X. Zou, W.M. Zhang, W.B. Li, K.X. Wei, Q.H. Gao, Z.K. Peng, G. Meng, Design and experimental investigation of a magnetically coupled vibration energy harvester using two inverted piezoelectric cantilever beams for rotational motion, *Energy Conv. Manage.* 148 (2017) 1391–1398.
- [44] Z. Yan, H. Lei, T. Tan, W. Sun, W. Huang, Nonlinear analysis for dual-frequency concurrent energy harvesting, *Mech. Syst. Signal Process.* 104 (2018) 514–535.
- [45] T. Tan, Z. Yan, W. Huang, Broadband design of hybrid piezoelectric energy harvester, *Int. J. Mech. Sci.* 131–132 (2017) 516–526.
- [46] T. Tan, Z. Yan, M. Hajji, Electromechanical decoupled model for cantilever-beam piezoelectric energy harvesters, *Appl. Phys. Lett.* 109 (2016), 101908.
- [47] A. Cammarano, S.A. Neild, S.G. Burrow, D.J. Inman, The bandwidth of optimized nonlinear vibration-based energy harvesters, *Smart Mater. Struct.* 23 (2014), 055019.

## Biographies



**Chung Ket Thein** graduated from University of Hull, UK with a bachelor degree and PhD in Mechanical Engineering in 2007 and 2011, respectively. He is currently an Assistant Professor in Heriot-Watt University Malaysia since 2016. His research interest includes multi-objective and multi-disciplinary optimisation and vibration energy harvesting devices for wireless sensor network applications.



**Faruq Muhammad Foong** is a Ph.D. candidate at the School of Mechanical Engineering, Heriot-Watt University Malaysia. He received his Bachelor of Aerospace Engineering degree (Hons) from Monash University, Australia. His research interest include energy harvesting, linear and non-linear vibrations. University, Putrajaya, Malaysia.



**Yi-Chung Shu** received the Ph.D. degree with major in Applied Mechanics and minor in Materials Science from the California Institute of Technology in 1998. He is now a Distinguished Professor at National Taiwan University and a faculty member of the Institute of Applied Mechanics. His research interest focuses on developing theoretical and numerical methods to study the behavior of smart materials at different length scales. He is also interested in the development of piezoelectric energy harvesting systems. Prof. Shu has been the recipient of the Outstanding Research Award from the National Science Council of Taiwan and Distinguished Young Scholar Award from the Society of Theoretical and Applied Mechanics.